MICAL2 is a novel nucleocytoplasmic shuttling protein promoting cancer invasion and growth of lung adenocarcinoma

Wolong Zhou, Yuanqi Liu, Yang Gao, Yuanda Cheng, Ruimin Chang, Xizhe Li, Yanwu Zhou, Shaoqiang Wang, Lubiao Liang, Chaojun Duan, Chunfang Zhang

PII: S0304-3835(20)30213-5

DOI: https://doi.org/10.1016/j.canlet.2020.04.019

Reference: CAN 114773

To appear in: *Cancer Letters*

Received Date: 13 November 2019

Revised Date: 2 April 2020

Accepted Date: 22 April 2020

Please cite this article as: W. Zhou, Y. Liu, Y. Gao, Y. Cheng, R. Chang, X. Li, Y. Zhou, S. Wang, L. Liang, C. Duan, C. Zhang, MICAL2 is a novel nucleocytoplasmic shuttling protein promoting cancer invasion and growth of lung adenocarcinoma, *Cancer Letters* (2020), doi: https://doi.org/10.1016/j.canlet.2020.04.019.

MICAL2 is a novel nucleocytoplasmic shuttling protein promoting cancer invasion and growth of lung adenocarcinoma

Wolong Zhou[1], Yuanqi Liu[1], Yang Gao[1], Yuanda Cheng[1], Ruimin Chang[1], Xizhe Li[1], Yanwu Zhou[1], Shaoqiang Wang[2], Lubiao Liang[3], Chaojun Duan[1, 4, *] and Chunfang Zhang[1,4,5, *]

1. Department of Thoracic Surgery, Xiangya Hospital, Central South University, Changsha, 410008, P.R. China.

2. Department of Thoracic Surgery, Affiliated Hospital of Jining Medical College, Jining Medical College, Jining, 272000, P.R. China.

3. Department of Thoracic Surgery, Affiliated Hospital of Zunyi Medical University, Zunyi Medical University, Zunyi, 563000, P.R. China.

4. National Clinical Research Center for Geriatric Disorders, Xiangya Hospital, Central South University, Changsha, 410008, P.R. China.

5. Hunan Engineering Research Center for Pulmonary Nodules Precise Diagnosis and Treatment, Xiangya Hospital, Central South University, Changsha, 410008, P.R. China.

*Corresponding address: Department of Thoracic Surgery, Xiangya Hospital, Central South University No.87, Xiangya Road, Changsha, Hunan 410008, P.R. China.

E-mail addresses: zcf6169@outlook.com (C. Zhang), duancjxy@126.com (C. Duan).

Abstract

MICAL2 is a tumor-promoting factor involved in cell migration, invasion, deformation, and proliferation not yet fully explored in lung adenocarcinoma (LUAD). This study demonstrated that MICAL2 was overexpressed and cytoplasm-enriched in LUAD tissues. Moreover, high cytoplasmic MICAL2 and/or total MICAL2 expression levels were positively correlated with lymphatic metastasis and shorter overall survival in LUAD patients. MICAL2 promoted LUAD cell proliferation, migration, invasion, and epithelial to mesenchymal transition—all of which involved the AKT and myosin-9 pathways. Furthermore, MICAL2 was identified as a nucleoplasm shuttling protein dependent on myosin-9 and its C-terminal fragment. MICAL2$^{-\Delta C}$—enriched in the nucleus—had less impact on tumor malignancy in LUAD cells *in vitro* and *in vivo*. Tumor promotion by MICAL2 was reduced by nuclear-export inhibitor, myosin-9 inhibitor, or si-myosin-9—all of which effectively inhibited MICAL2's nuclear export. Finally, the expression and subcellular location as well as clinical significance of MICAL2 and myosin-9 were analyzed across TCGA data and LUAD tissue arrays. Our data revealed that MICAL2 overexpression and nuclear export were associated with cancer progression; inhibiting its expression and/or nuclear export may provide a new target for LUAD therapy.

Keywords

MICAL-2, nucleoplasm shuttling protein, EMT, *MYH9*, LUAD

1. Introduction

Lung cancer is the most frequently diagnosed cancer and the leading cause of death from cancer worldwide, accounting for nearly 13% of all cancer diagnoses and approximately 19% of total cancer deaths [1]. Lung adenocarcinoma (LUAD) accounts for approximately 40% of lung cancers. Although surgery and chemotherapy offer remarkable therapeutic effects in early stage LUAD, late stage and metastatic LUADs are challenging based on their unresectable properties and drug-resistant tendencies. Advances in research offer insight into the molecular and cell-biological changes involved in metastasis [2]; the investigation of such factors is essential for developing new therapies as well as providing potential novel biomarkers for LUAD [3].

The family of molecules interacting with CasL (MICAL)—characterized by the N-terminal flavoprotein mono-oxygenase (MO) domain [4]—is involved in vesicle trafficking, cytoskeleton remodeling, autophagy and phagocytosis, cell division, cell movement, cell proliferation, axon guidance, and angiogenesis [5,6,7,8,9,10]. MICAL2 is a special member of the MICALs family—the activation of which is not inhibited by self-inhibitory activity [11]— that has been identified as a tumor promoter in several cancers including prostate [12], gastric [13], breast [14], and colorectal [15]. MICAL2 directly binds to and disassembles F-actin [9], regulates SRF signaling [16], stabilizes

EGFR protein [14], mediates P53 ubiquitin[15], and promotes EMT through various pathways [9,17,18]. Although it is reportedly enriched in the nuclei of HEK293T, COS7, and HeLa cells [16] and in colorectal cancers [15], the subcellular localization of MICAL2 is not fully defined. Other articles report cytoplasmic enrichment in HeLa cells [19], neoplastic emboli [18], and activated endothelial cells of blood vessels [20]. Certain studies also showed MICAL2 diffusely located in both the nucleus and the cytoplasm [14,18]. However, the expression pattern and role of MICAL2 in LUAD have not been thoroughly explored.

In the present study, the expression and distribution of MICAL2 were analyzed in LUAD tissue arrays, as well as its relationship with the clinicopathological characteristics of LUAD patients. Cell experiments revealed tumor-promoting effects (growth, invasion, and EMT) involving MICAL2 pathways in LUAD cell lines. Furthermore, our findings identified MICAL2 as a nucleocytoplasmic shuttling protein. Finally, the regulation and cytological function of MICAL2 nuclear export were investigated both *in vitro* and *in vivo*.

2. Materials and Methods

2.1 Tissue specimens

Paired human tumor/normal tissue samples were collected from June 2004 through

September 2015 (first collection, n = 126), with follow-up for 4 to 5 years after surgery. The second round (n = 74) of LUAD tissue samples were collected from April 2014 to January 2018. Pathological diagnosis was rendered by experienced pathologists. Upon the approval of the relevant ethics committee of Xiangya Hospital of Central South University and written consent from patients, samples were collected in the operating room, formalin fixed, and embedded in paraffin. The paired normal tissue was collected more than 10 cm from the tumor edge. Two hundred pairs of LUAD samples were ultimately appropriated for the study, from patients with an average age of 57 (ranging from 20 to 84 years): 87 were from female patients and 113 were from male patients; 81 contained lymph node metastases; 86 cases were in stage I, 46 were in stage II, 68 were no less than stage III. We excluded sub-standard cases such as patients who had undergone pre-operative radiotherapy or chemotherapy, as well as those with lung squamous cell carcinoma or benign tumors.

2.2 Cell lines and culture

PC9, A549, BEAS-2B, LTEP-α-1, HeLa, and HEK293T cells were authenticated via short tandem repeat (STR) analysis. All cell lines were passaged less than 10 times after their initial revival from frozen stocks. The cells were cultured in RPMI-1640 or DMEM (for HEK293T cells only) growth medium (Gibco/Thermo Fisher Scientific, Waltham, MA, USA) with 10% fetal bovine serum (FBS; Gibco). The cell culture

incubator was set at 37 ℃ with 5% CO_2.

2.3 Immunohistochemistry (IHC)

Sample slides with 3-μm thick tissue sections were deparaffined in xylene, rehydrated in descending concentrations of ethanol and PBS, and subjected to epitope retrieval by citrate buffer (pH 6.0). Endogenous peroxidases were blocked by 3% hydrogen peroxide in methanol. Slides were then incubated overnight in the indicated antibodies [rabbit anti-MICAL2 (1:50; Abnova, Taipei, Taiwan); rabbit anti-Flag (1:200; Proteintech, Rosemont, IL, USA); rabbit anti-myosin-9 (1:400; Proteintech)] at 4 ℃ followed by 15 min at 20 ℃, then in biotin-conjugated goat anti-rabbit antibody (1:200; Vector® Laboratories, Burlingame, CA, USA) for 1 h at 20 ℃, in ABC HRP reagent (Vector®) for 1 h at 20 ℃ and DAB Peroxidase Substrate Kit (Vector®) for approximately 3 min in the dark. Positive (hepatic tissue) and negative controls were assayed at the same time. Results were obtained on an Aperio digital pathology slide scanner (Leica Biosystems, Nußloch, Germany) and a Leica DM6B microscope (Leica Microsystems, Wetzlar, Germany). Staining was evaluated based on both mean integrated optical density (MI = IOD/AREA) [21,22] using the Image-Pro Plus 6.0 application (Media Cybernetics, Inc., Rockville, MD, USA) for overall staining and a binary system for nuclear or cytoplasmic staining termed the immunoreactive score (IRS = SI <staining intensity> × PP <percentage of positive cells>). Kaplan-Meier analysis was conducted using the average MI value cut-off

which divided slices into high expression and low expression groups [23]. SI was classified as follows: 0, negative; 1, weak; 2, moderate; and 3, strong. PP was defined as follows: 0, negative; 1, 1–10% positive cells; 2, 11–50% positive cells; 3, 51–80% positive cells; and 4, more than 80% positive cells. Slices scoring no less than 4 points were classified as immunoreactive [24,25].

2.4 Plasmids and constructs

The shMICAL2s were synthesized and purified by Hanyin Biotech Co. (Shanghai, China) and integrated into pHY-023 vector (Hanyin Biotech), targeting *MICAL2* with the following primers: 5'-CCTCCAGGCCTTCAACATT-3', 5'-CCAAAGCCCTGTG GTACAA-3', 5'-GCGCACTGCCATTGAACTT-3'. Constructs containing human MICAL2-Flag fusions were integrated into pHY-023 and GV141 vectors (Genechem, Sha nghai, China). Coding sequences of truncated mutants of MICAL2 were obtain ed using specific primers: MICAL2$^{-\Delta C}$: 5'-ACGGGCCCTCATGGGGGAAAACGAGGATG AGAAGCAG-3' and 5'-CCAAGCTTGGCTGCTTCATGAGTGAGGGGTT-3'; MICAL2$^{-\Delta N}$: 5'-ACGGGCCCTCATGAACAAACGGAGACGGAAGGGCTTCA-3' and 5'-TTAAGCTTGGGCCAA GAAGTGGGTGTAGCACTGGAAG-3'; MICAL2$^{-\Delta N\Delta C}$: 5'-ACGGGCCCTCATGCTGGGAGTTGA AATCCATGTG-3' and 5'-CCAAGCTTGGCTGCTTCATGAGTGAGGGGTT-3'. The pENTER-Myosin9-Flag/His plasmid was purchased from Vigene Bioscience (Shandong, C hina). Both MICAL2-HA and myosin9-HA were subcloned from Flag-tagged plas mid into GV366 plasmid (Genechem) using XbaI (TaKaRa, Shiga, Japan) and N otI (TaKaRa). All gene cloning was verified by sequencing. The *MYH9* siRNAs

were synthesized by Guangzhou RiboBio Co. (Guangzhou, China) targeting *MYH9* with the following primers: 5'-GCATCAACTTTGATGTCAA-3', 5'-GCAACACGGAG CTGATCAA-3'.

2.5 Western blotting and immunoprecipitation

Western blotting (WB) was performed according to standard protocols using 10% Bis-Tris gels. Membranes were incubated in primary antibodies [rabbit anti-MICAL2, 1:1000 (Abnova); rabbit anti-ZO1, 1:1000 (Abcam, Cambridge, UK); rabbit anti-E cadherin, 1:200 (Abcam); rabbit anti-β catenin, 1:3000 (Abcam); rabbit anti-vimentin, 1:3000 (Abcam); rabbit anti-*MYH9*, 1:2000 (Proteintech); rabbit anti-AKT, 1:3000 (Cell Signaling Technology, CST, Danvers, MA, USA); rabbit anti-AKT(Ser473), 1:3000 (CST); rabbit anti-GSK-3β, 1:1000 (CST); rabbit anti-GSK-3β(Ser9), 1:1000 (CST); mouse anti-Flag, 1:4000 (MilliporeSigma, Burlington, MA, USA); mouse anti-HA, 1:500 (Santa Cruz Biotechnology, Dallas, TX, USA)] overnight at 4 ℃. Immunoprecipitation was performed as described previously [26] using EZview™ Red ANTI-FLAG® M2 Affinity Gel (MilliporeSigma) overnight at 4 ℃.

2.6 immunofluorescence

Primary antibodies for immunofluorescence (IF) were sourced as follows: anti-MICAL2 from Abnova; monoclonal anti-Flag M2 from Sigma-Aldrich (St. Louis,

MO, USA). Treatment: PC-9 cells or A549-MICAL2 cells were treated with or without 10 nM LMB (leptomycin B; CST) or 10 μM ML7 (myosin-9 inhibitor; Selleck Chemicals, Houston, TX, USA) overnight, then harvested for detection of MICAL2 localization by indirect immunofluorescence using anti-MICAL2 antibody or anti-Flag antibody followed by Alexa Fluor®-conjugated secondary antibody (green; Abcam). They were then scanned with a confocal imaging system (Leica SP8) or fluorescence microscope (Leica DM LB2).

2.7 Cell proliferation assays

Cell proliferation was detected using the CCK-8 (Cell Counting Kit-8; Dojindo, Kumamoto, Japan) method and a plate clone formation assay. For the CCK-8 assay, 2000 cells per well were seeded in 96-well plates and absorbance was read at 450 nm at 6, 24, 48, and 72–96 h, respectively, after being incubated with CCK-8 for 2 h. For the plate clone formation assay, 600 cells were seeded in 10 cm dishes (or 200 cells in a 6-well plate) and stained with 0.05% crystal violet after 2 to 3 weeks of cell culture.

2.8 Cell migration and cell invasion assays

For the cell migration assay, 3×10^4 cells were seeded into the upper chamber of a collagen-precoated transwell filter (8 μm pores; Costar, Acton, MA, USA) with

RPMI-1640 medium without FBS. RPMI-1640 medium containing 15% FBS was added to the lower chamber. The plates were maintained in the cell culture incubator overnight. After being fixed by methanol and stained with 0.05% crystal violet, four different areas (up, down, left, and right) of the plates were imaged using an optical microscope (Leica DMi1). For the cell invasion assay, 5×10^4 cells per well were seeded into the upper chamber of a Matrigel-precoated transwell filter (8 μm pores; Costar) or a transwell filter (8 μm pores; BD, Franklin Lakes, NJ, USA) coated with 100 μl of 300 μl/ml Matrigel (BD).

2.9 Immunoprecipitation mass spectrometry (IP-MS)

PC-9 cell lysis solution was assessed to investigate the binding protein of endogenic MICAL2. The antibody used for immunoprecipitation was rabbit polyclonal anti-MICAL2 (1:100; Proteintech). Sequencing-grade trypsin (Promega, Madison, WI, USA) was used for tryptic digestion. One-half of the volume of each sample was separated and analyzed with an EASY-nLC™ 1200 nano-UPLC coupled to a Q Exactive™ mass spectrometer (Thermo Finnigan/Thermo Fisher Scientific, San Jose, CA, USA). Separation was performed using a reversed-phase column (100 μm, ID × 15 cm, Reprosil-Pur 120 C18-AQ, 1.9 μm; Thermo Fisher Scientific). Data-dependent acquisition was performed in profile and positive modes on an Orbitrap analyzer (Thermo Fisher Scientific). Potential MICAL2-binding proteins were selected by intensity ratios > 10 (MICAL2-Ab: IgG > 10). The false discovery rate (FDR) was

analyzed by performing a concatenated decoy database search and the identified proteins were reported at FDR < 1%.

2.10 Immunoprecipitation parallel reaction monitoring (IP-PRM)

PC-9 cell lysis solution was used to test the binding interaction between endogenous myosin-9 and MICAL2. Rabbit polyclonal anti-*MYH9* antibody (1:1000; Proteintech) was used for IP. After tryptic digestion, 2 μg peptide was separated on an EASY-nLC™ 1200 nano-UPLC coupled to the Q Exactive™ mass spectrometer system mentioned above (Thermo Finnigan). Data-dependent acquisition was performed in profile and positive modes on the Orbitrap analyzer (Thermo Fisher Scientific). The collected PRM data were imported into Skyline for peptide matching [27].

2.11 Tumor xenograft model

For the *in vivo* tumor metastasis assay, 1×10^6 A549 cells stably expressing MICAL2-Flag, MICAL2$^{-\Delta C}$-Flag or vector-CTRL were injected into the tail veins of female BABL/c athymic nude mice (age 4–5 weeks). After 5 weeks, all animals were sacrificed. The lung tissues were excised and fixed in formalin. Hematoxylin and eosin (H&E) staining was performed to detect metastatic focus and IHC to detect MICAL2-Flag or MICAL2$^{-\Delta C}$-Flag expression levels. All animal experiments were approved by the Central South University Animal Care Commission.

2.12 Analysis of LUAD data sets

RNA sequencing data from The Cancer Genome Atlas (TCGA) LUAD (706 samples) were obtained from the University of California, Santa Cruz, Xena browser (UCSC Xena, https://xenabrowser.net/). Pearson's correlation was computed among features using log-transformed expression values.

2.13 Statistical Analysis

Statistical differences between two groups were tested using Student's t-test. Comparisons among three or more groups were conducted using one-way ANOVA. The chi-squared test was used to evaluate the significance of correlation. Survival analysis was performed using the Kaplan–Meier method. *P*-values < 0.05 were considered statistically significant (*, $P < 0.05$; **, $P < 0.01$; ***, $P < 0.001$; ****, $P < 0.0001$). Correlation between MICAL2 and myosin-9 in LUAD tissue arrays was analyzed using nonparametric Spearman correlation. Error bars represent standard error of the mean. All calculations were performed with SPSS Version 20.0 (IBM Corp., Armonk, NY, USA) or GraphPad Prism 6.01 (GraphPad Software Inc., San Diego, CA, USA).

3. Results

3.1 MICAL2 was overexpressed and cytoplasm-enriched in LUADs compared to normal lung tissues

To assess MICAL2 expression patterns in LUADs, IHC was performed on human LUAD tissue arrays containing 126 individual LUADs and the paired normal lung tissues. MICAL2 expression was detected solely in the nucleus of approximately 62% of normal lung tissues, while it was expressed in the nucleus and/or cytoplasm in approximately 84% of LUADs (Fig. 1A). We then compared the total expression of MICAL2 by comparing the mean integrated optical density (MI) of MICAL2 using Image-Pro Plus 6.0 software. The average MI for MICAL2 expression in LUADs was 0.106 ± 0.049, which was much higher than that in normal lung tissues (0.037 ± 0.027; $P < 0.0001$; Fig. 1A). Compared with the matched normal lung tissues, the expression levels of nuclear MICAL2 in LUADs were dramatically decreased in 74 of 126 (58.7%) cases while cytoplasmic MICAL2 increased in 124 of 126 (98.4%) cases ($P < 0.0001$; Fig. 1A). Together, MICAL2 was overexpressed and nuclear exported in LUAD tissues.

3.2 High cytoplasmic MICAL2 or total MICAL2 expression positively correlated with lymphatic metastasis and poor prognosis in LUADs

The different expression patterns of MICAL2 in LUADs and paired normal lung tissues

led us to further analyze the relationship between clinicopathological characteristics and MICAL2 expression levels and subcellular location. As shown in Table 1 and Figure 1B, both the overall expression and the cytoplasmic translocation of MICAL2 in the primary LUADs were positively associated with lymph node metastasis ($P < 0.05$ and $P < 0.0001$, respectively) and advanced TNM stage ($P < 0.05$ and $P < 0.01$, respectively). In contrast, MICAL2 expression levels were not associated with gender, age, tumor size, or differentiation (Table 1). Accordingly, high levels of total and cytoplasmic MICAL2 expression were correlated with poor overall survival (OS) in LUAD patients (Fig. 1C; $P < 0.05$).

3.3 MICAL2 promoted LUAD cell proliferation, migration, invasion, and epithelial to mesenchymal transition

Given that MICAL2 was overexpressed in the LUAD tissues, we next investigated MICAL2 function in LUAD cell lines. Western blotting revealed that MICAL2 was highly expressed in PC-9, BEAS-2B, and HTB-182 cells, but not in A549, H446, and LTEP-α-2 cells (Fig. 2A). Based on these results, knockdown of MICAL2 was performed in the MICAL2-high PC-9 cell line using three independent shRNAs. We confirmed significant knockdown in two—namely, the PC-9_sh1 and PC-9_sh3 cells (Fig. 2B, C). Knockdown of MICAL2 greatly inhibited the proliferation, migration, and invasion of PC-9 cells (Fig. 2C-E). Knockdown of MICAL2 also induced significant morphological changes in the PC-9 cells, leading to the formation of cobble stone-like

cells and a reduction in protuberances indicating mesenchymal to epithelial transition (MET) (Fig. 2F, 2C, S1). Consistent with this, knockdown of MICAL2 led to reduced expression of the mesenchymal markers vimentin and β-catenin and increased expression of the epithelial markers ZO-1 and E-cadherin (Fig. 2G). Cell signaling pathways responsible for eliciting EMT and cell proliferation and migration converge on AKT and myosin-9. Reduced expression of myosin-9 and repressed phosphorylation of AKT and GSK-3β in the MICAL2-knockdown PC-9 cells were confirmed, indicating the potential role of these signaling pathways in mediating MICAL2 function in LUADs (Fig. 2G).

To further verify the tumor promoting role of MICAL2 in LUADs, a lentiviral gene delivery system was used to overexpress MICAL2 in the MICAL2-low A549 cells with undetectable levels of endogenous MICAL2 expression (Fig. 2A, 2B). CCK8 and plate clone assays illustrated that MICAL2 promoted A549 cell proliferation (Fig. 2C, 2D). Transwell assays further revealed that MICAL2 enhanced the migration and invasion abilities of A549 cells (Fig. 2E). MICAL2-overexpressing A549 cells also exhibited mesenchymal-like phenotype with longer and more numerous protuberances (Fig. 2F, 2C, S1). Accordingly, western blotting confirmed the increased expression of the EMT markers vimentin and β-catenin and the decreased expression of ZO-1 and E-cadherin (Fig. 2G). Interestingly, myosin-9 expression and phosphorylation of AKT and GSK-3β were significantly increased in the MICAL2-overexpressing A549 cells (Fig. 2G). Altogether, these data suggest that MICAL2 promotes tumor malignancy and

induces EMT in LUAD cells along with increased levels of myosin-9 expression and AKT phosphorylation.

3.4 MICAL2 was sensitive to LMB and relied on its C-terminal end to shuttle between the cytoplasm and the nucleus

To further understand how MICAL2 works in LUADs, the subcellular location of MICAL2 was investigated. These localizations have been reported disparately for different cell lines [14,15] or even for the same cell lines in different articles [16,19]. MICAL2 expression patterns varied in LUADs (Fig. 1), with a similar situation observed in LUAD cell lines (data not shown). This raises the question whether MICAL2 actively shuttles between the cytoplasm and nucleus in LUAD cells. Given that proteins larger than 40–60 kDa (full length of MICAL2, 127kDa) barely diffuse freely through nuclear pores and that the MICAL2 protein contains a nuclear localization sequence (NLS) [28], we sought to determine whether the blockage of active nuclear export by leptomycin B (LMB)—an inhibitor of export receptor chromosome maintenance region 1 [29]—affects MICAL2 cellular translocation. The immunofluorescence assay followed by confocal imaging confirmed that LMB blocked the nuclear export of endogenous MICAL2, leading to nuclear accumulation in the PC-9 cells (Fig. 3A). A similar observation was made for ectopically overexpressed MICAL2 in the A549 cells (Fig. 3B). This indicated that MICAL2 is a nucleocytoplasmic shuttling protein, dependent on the exportin 1 nuclear export receptor.

MICAL2 contains a kinase domain (the MO domain), an actin-binding domain (the CH domain), a previously identified NLS, and a LIM domain [9,16]. Given that NLSs and NESs (nuclear export signals) are generally required for the active nuclear-cytoplasmic trafficking of proteins [28], we attempted to allocate the NESs within MICAL2. We made several truncation mutants of Flag-tagged MICAL2 including MICAL2$^{-\Delta C}$, MICAL2$^{-\Delta N\Delta C}$, and MICAL2$^{-\Delta N}$ (Fig. 3C) and transfected them into HeLa cells. Then immunofluorescence was performed using anti-Flag antibody to detect the subcellular location of MICAL2 mutants. As shown in Fig. 3C, while MICAL2$^{-\Delta N}$ with the deletion of both the MO and CH domains exhibited a dispersed distribution throughout the cells similar to wild type MICAL2 (MICAL2-WT), MICAL2$^{-\Delta C}$ and MICAL2$^{-\Delta N\Delta C}$ predominantly localized in the nucleus. Furthermore, there was no statistical difference in the cytoplasmic positive rate between MICAL2$^{-\Delta C}$ and MICAL2$^{-\Delta N\Delta C}$, suggesting that the C-terminal fragment of MICAL2 contains the NESs for actively exporting MICAL2. Moreover, MICAL2$^{-\Delta C}$ without the loss of the MO domain (kinase domain) and CH domain (actin-binding domain) provides a useful framework to investigate the functional contribution of MICAL2 in the nucleus.

3.5 MICAL2 nuclear export depended on myosin-9 in LUAD cells

To further investigate the factors mediating the nucleocytoplasmic shuttling of MICAL2, immunoprecipitation (using anti-MICAL2 antibody) coupled with mass

spectrometry (IP-MS) was applied to search for the endogenous MICAL2-binding proteins in PC-9 cells. After subtracting the non-specific binding proteins using isotype-controlled IP-MS, 108 proteins were identified as MICAL2-binding partners with intensity ratios > 10 (MICAL2-Ab: IgG > 10, data not shown). The FDR was analyzed by performing a concatenated decoy database search and the identified proteins were reported at FDR < 1%. Myosin-9 (*MYH9*)—a motor protein associated with certain nucleocytoplasmic shuttling proteins [30,31,32,33,34]—was among the top-five MICAL2-binding proteins ranked by intensity ratio (Fig. 4A, Table S1). We further performed immunoprecipitation (using anti-myosin-9 antibody) coupled with a parallel reaction monitoring assay (IP-PRM) and confirmed endogenous MICAL2-myosin-9 interaction in the PC-9 cells (Fig. 4B). In addition, exogenous MICAL2 and myosin-9 binding was identified by a co-IP assay in HEK293T cells (Fig. 4C). The co-IP assay also showed that si-myosin-9 negatively affected myosin-9 expression levels as well as binding capacity to MICAL2 (Fig. 4C). Next, to determine whether myosin-9 affects the subcellular location of MICAL2 in LUAD cells, A549-MICAL2 cells were treated with ML7—a myosin-9 specific inhibitor—and si-myosin-9. Immunofluorescence assays revealed that both ML7 and si-myosin-9 treatment led to the nuclear accumulation of MICAL2 (Fig. 4D). Altogether, these data suggest that myosin-9 binds to MICAL2 and promotes MICAL2 nuclear export.

3.6 The cytoplasmic translocation of MICAL2 was required for its cancer-promoting activity *in vitro* and *in vivo*

The data described above revealed that MICAL2 is a tumor promoter in LUADs as well as a nucleocytoplasmic shuttling protein that is sensitive to LMB, ML7, and si-myosin-9 treatments. Moreover, the MICAL2 C-terminal fragment contains the candidate NES sequence(s) for nuclear export. To investigate whether the cellular location of MICAL2 determines its cancer-promoting activity in LUAD cells, we examined how LMB, ML7 and si-myosin-9 treatments and the deletion of the C-terminal fragment affect MICAL2 tumor-promoting activities in LUAD.

A lentiviral approach was used to generate the A549 cells with overexpression of wild type MICAL2 (MICAL2-WT), MICAL2$^{-\Delta C}$, or control (Ctrl, Fig. 5A). Both MICAL2-WT and MICAL2$^{-\Delta C}$ induced myosin-9 upregulation (Fig. 5A). The CCK8 assays revealed that MICAL2$^{-\Delta C}$ exhibits only minimal tumor-promoting activity that is still significantly higher than that of the Ctrl but much lower than that of wild type MICAL2 (Fig. 5B). In contrast, MICAL2$^{-\Delta C}$ completely lost its capacity to promote cell migration and invasion (Fig. 5C). This lack of migration/invasion-promoting activity is likely due to the mislocation but not misfolding of the MICAL2$^{-\Delta C}$ protein, given that this protein maintained its ability to induce myosin-9 expression as well as weakly promoted cell proliferation. To investigate the effect of MICAL2 and its nuclear export on the metastasis potential of LUAD cells *in vivo*, 1×10^6 A549-CTRL, A549-MICAL2$^{-\Delta C}$, or A549-MICAL2 cells were injected into the tail veins of nude mice. H&E staining showed increased metastatic nodule numbers in A549-MICAL2 cells but not

A549-MICAL2$^{-\Delta C}$ compared with A549-CTRL cells (Fig. 5D).

Finally, blocking MICAL2 cytoplasmic translocation using LMB, ML7, or si-myosin-9 robustly blocked MICAL2 capacity to drive cell proliferation, motility, and invasion (Fig. 6). This further supports the premise that cytoplasmic MICAL2 exerts LUAD-promoting activity, which may functionally explain the different cellular locations of MICAL2 in LUADs and normal lung tissues.

3.7 Expression of MICAL2 and myosin-9 in LUAD tissues.

In order to confirm the correlation between MICAL2 and myosin-9 revealed in the cell experiment, their expression levels were determined in LUAD tissues. TCGA data showed that the mRNA levels of *MICAL2* and *MYH9* were in accordance (n = 706, r = 0.5104, $P < 0.0001$) (Fig. S2A). Then IHC of LUAD tissue arrays was performed for further exploration (Fig. S2B). The protein levels of total and cytoplasmic MICAL2 were positively corelated with myosin-9. In addition, the subcellular location of MICAL2 and myosin-9 were also in accordance, which forms the basis of their binding capacity in LUADs. Furthermore, only double-positive staining of MICAL2 and myosin-9 was positively associated with lymph node metastasis (Table S2). Overall, our results suggest that MICAL2 and myosin-9 might synergistically contribute to LUAD metastasis.

4. Discussion

Lung cancer is the leading cause of cancer-related mortality worldwide [35]. Metastasis is the most critical parameter determining survival in lung cancer cases [36]. Therefore, the identification of novel prognostic biomarkers and treatment targets of metastatic lung cancer is urgent for patients. In the current study, we identified a novel role of subcellular MICAL2 in the prognosis of LUAD as well as its nucleocytoplasmic shuttling and tumor-promoting action in LUAD cell lines.

MICAL2 levels were overexpressed in cancers such as prostate cancer [37], gastric carcinoma [18], breast cancer [14], and colorectal cancer [15]. However, the prognostic and predictive value of MICAL2 expression levels for LUADs remains unclear. In the current study, MICAL2 was overexpressed and nuclear exported in LUADs compared to the adjacent normal lung tissues (Fig. 1). Furthermore, our results indicated that both overall levels and cytoplasmic levels of MICAL2 contributed to LUAD lymphatic metastasis and shorter OS (Table 1). These significant differences in MICAL2 between LUAD tissues and normal lung tissues along with its predictive value in LUAD patients make MICAL2 an ideal candidate as a cancer biomarker.

To assess the oncogenic activity of MICAL2, the role of MICAL2 in LUAD cell lines was explored. MICAL2 has been described as a tumor promoter via various signal

pathways [9,17]. However, MICAL2 had yet to be explored in LUAD cell lines. In our study, MICAL2 was found to be necessary for cell proliferation, migration, invasion, and EMT changes in LUAD cell lines via the AKT and myosin-9 pathways. Given that MICAL2 activates SRF signaling through redox-dependent depolymerization of nuclear actin [16] and SRF binds to the CArG box located at the *MYH9* promoter [38], we propose that MICAL2 promotes *MYH9* expression. Surprisingly, *MYH9* expression levels are corelated with MICAL2 expression levels as well as MICAL2$^{-\Delta C}$ in LUAD cell lines (Fig. 2G, 5A), which is confirmed in TCGA data and tissue arrays (Fig. S2). Moreover, myosin-9 was identified as a tumor promoter in NSLCs (non-small cell lung cancer); it was overexpressed and significantly corelated with lymphatic invasion and poor prognosis [39]. In addition, several articles report that myosin-9 promoted tumorigenesis by regulating AKT signaling [40,41,42,43]. AKT is a key signaling node connecting oncogenic proteins to tumor-promoting effects in lung cancers [44,45,46,47]. In the present study, MICAL2 was corelated with myosin-9 expression and p-AKT levels (Fig. 2G). Our study also showed that myosin-9 bound to MICAL2 and promoted MICAL2 nuclear export (Fig. 4), which facilitated MICAL2's participation in oncogenic processes. This also reduced the influence of MICAL2 in the nucleus, which may in turn have prevented excessive *MYH9* expression. In short, the MICAL2-SRF-*MYH9*-AKT pathway may exist in LUAD cell lines and might be self-regulated by myosin-9's promotion of MICAL2 nuclear export. Nevertheless, more evidence is needed to draw this conclusion.

The subcellular location of proteins is an essential factor determining the efficiency of various biological processes [48]. In this study, MICAL2 was determined to be a nucleoplasm shuttling protein, relying on its C-terminal end and myosin-9 while being sensitive to LMB and ML7. Furthermore, its nuclear export is necessary for its tumor-promoting effect. Myosin-9 inhibitor together with a short chain polypeptide targeting the NES of MICAL2 might be an alternate strategy for inhibiting the carcinogenesis of MICAL2.

The mechanisms by which nuclear-exported MICAL2 affects cell migration capacity vary. First, MICAL2 directly binds and disassembles F-actin as an oxidation-reduction enzyme [9,10,19]. Cytoplasmic MICAL2 is colocalized with F-actin at the edge of lamellipodia [18,19]. Accordingly, migration and invasion abilities were strongly inhibited with the depletion of cytoplasmic MICAL2 in LUAD cells (Fig. 6). In addition, myosin-9 is overexpressed in lung cancers and attenuates NSLC metastasis [39,49]. In the present study, MICAL2$^{-\Delta C}$—enriched in the nucleus—led to higher levels of myosin-9 expression (Fig. 5A), while it had no significant effect on cell motility in LUAD cells (Fig. 6C, D). On one hand, this indicates that cytoplasmic MICAL2 is crucial for its motility-promoting effect in LUADs. On the other hand, it raises the possibility that myosin-9 promotes cancer metastasis through MICAL2 in LUADs. First, the redox-regulation of myosin-9 results in microfilament remodeling and altered cellular motility [50]. Given that MICAL2 is a redox enzyme [9,51] and that myosin-9 was shown to bind MICAL2 (Fig. 4), further study could focus on whether MICAL2 can

redox myosin-9 regulating microfilament depolymerization. Secondly, myosin filament organization is regulated by small Rho GTPases [52] and the activation of Rac1 (a member of the Rho family) is affected by MICAL2 [14]; thus, MICAL2 can also regulate myosin-9 through Rac1. Thirdly, myosin-9 is reportedly involved in lamellipodia extension based on its assembly regulation or as an ABP (actin-binding protein) regulating the actin network [53]. Given that MICAL2 can directly depolymerize F-actin [19] and improve the binding of cofilin (an ABP) to filaments [54], it is possible that MICAL2 also regulates F-actin and promotes lamellipodia formation through myosin-9. Altogether, the regulation between MICAL2 and myosin-9 is mutual, variable, and acts in stereo, leading to cell migration and tumor metastasis. Consequently, future studies should explore the synergistic anti-tumor activity that ensues when pairing MICAL2 inhibitors with myosin-9 inhibitors.

In summary, our research demonstrates that subcellular MICAL2 expression levels are significantly correlated with prognosis in LUAD patients and play an important role in LUAD cell proliferation and invasion. MICAL2 is a nuclear-cytoplasmic shuttling protein in LUAD cells which relies on its C-terminal fragment as well as myosin-9. Applying LMB, ML7, or si-myosin-9 or deleting the C-terminal end of MICAL2 inhibits its nuclear export as well as its carcinogenic effects. This study contributes to our ever-increasing understanding of the subcellular distribution and carcinogenicity of MICAL2 and suggests that MICAL2 is a promising cancer marker candidate and therapeutic target for LUAD.

Conflicts of interest

The authors declare that they have no conflicts of interest.

Acknowledgements

Our sincere appreciation goes out to all members of the Feng Yang lab for providing language assistance and technical guidance. Thank you to Wuyang Zhang and Jun Su for their language assistance. Thank you to Liuliu and all other family members for their encouragement and support.

Funding sources

This work was supported by the National Natural Science Foundation of China Grants (Nos. 81372515, 81572281, 81702278, 81401901, 81802290, and 81974367), Innovation Programme of Central South University (2020 CX043) and Scientific Assignment of Hunan Health Commission (C2019185).

References:

[1] L.A. Torre, F. Bray, R.L. Siegel, J. Ferlay, J. Lortet-Tieulent, A. Jemal, Global cancer statistics, 2012. CA: A Cancer Journal for Clinicians 65 (2015) 87-108.

[2] S. Valastyan, R.A. Weinberg, Tumor metastasis: molecular insights and evolving paradigms. Cell 147 (2011) 275-92.

[3] D.X. Nguyen, J. Massague, Genetic determinants of cancer metastasis. Nat Rev Genet 8 (2007) 341-52.

[4] M. Nadella, M.A. Bianchet, S.B. Gabelli, J. Barrila, L.M. Amzel, Structure and activity of the axon guidance protein MICAL. Proc Natl Acad Sci U S A 102 (2005) 16830-5.

[5] S.M. Kolk, R.J. Pasterkamp, MICAL flavoprotein monooxygenases: structure, function and role in semaphorin signaling. Adv Exp Med Biol 600 (2007) 38-51.

[6] Y. Cai, J. Lu, F. Tang, Overexpression of MICAL2, a novel tumor-promoting factor, accelerates tumor progression through regulating cell proliferation and EMT. J Cancer 9 (2018) 521-527.

[7] J. Fischer, T. Weide, A. Barnekow, The MICAL proteins and rab1: a possible link to the cytoskeleton? Biochem Bioph Res Co 328 (2005) 415-423.

[8] B.C. Lee, Z. Péterfi, F.W. Hoffmann, R.E. Moore, A. Kaya, A. Avanesov, et al., MsrB1 and MICALs Regulate Actin Assembly and Macrophage Function via Reversible Stereoselective Methionine Oxidation. Mol Cell 51 (2013) 397-404.

[9] L.T. Alto, J.R. Terman, MICALs. Curr Biol 28 (2018) R538-R541.

[10] S. Frémont, G. Romet-Lemonne, A. Houdusse, A. Echard, Emerging roles of MICAL family proteins – from actin oxidation to membrane trafficking during cytokinesis. J Cell Sci 130 (2017) 1509-1517.

[11] S.S. Giridharan, J.L. Rohn, N. Naslavsky, S. Caplan, Differential regulation of actin microfilaments by human MICAL proteins. J Cell Sci 125 (2012) 614-24.

[12] S. Ashida, M. Furihata, T. Katagiri, K. Tamura, Y. Anazawa, H. Yoshioka, et al., Expression of novel molecules, MICAL2-PV (MICAL2 prostate cancer variants), increases with high Gleason score and prostate cancer progression. Clin Cancer Res 12 (2006) 2767-73.

[13] S. Mariotti, I. Barravecchia, C. Vindigni, A. Pucci, M. Balsamo, R. Libro, et al., MICAL2 is a novel human cancer gene controlling mesenchymal to epithelial transition involved in cancer growth and invasion. Oncotarget 7 (2016) 1808-25.

[14] Y. Wang, W. Deng, Y. Zhang, S. Sun, S. Zhao, Y. Chen, et al., MICAL2 promotes breast cancer cell migration by maintaining epidermal growth factor receptor (EGFR) stability and EGFR/P38 signalling activation. Acta Physiol 222 (2018) e12920.

[15] J. Lu, Y. Li, Y. Wu, S. Zhou, C. Duan, Z. Dong, et al., MICAL2 Mediates p53 Ubiquitin Degradation through Oxidating p53 Methionine 40 and 160 and Promotes Colorectal Cancer Malignance. Theranostics 8 (2018) 5289-5306.

[16] M.R. Lundquist, A.J. Storaska, T. Liu, S.D. Larsen, T. Evans, R.R. Neubig, et al., Redox Modification of Nuclear Actin by MICAL-2 Regulates SRF Signaling. Cell 156 (2014) 563-576.

[17] Y. Cai, J. Lu, F. Tang, Overexpression of MICAL2, a novel tumor-promoting factor, accelerates tumor progression through regulating cell proliferation and EMT. J Cancer 9 (2018) 521-527.

[18] S. Mariotti, I. Barravecchia, C. Vindigni, A. Pucci, M. Balsamo, R. Libro, et al., MICAL2 is a novel human cancer gene controlling mesenchymal to epithelial transition involved in cancer growth and invasion. Oncotarget 7 (2016) 1808-25.

[19] S.S.P. Giridharan, J.L. Rohn, N. Naslavsky, S. Caplan, Differential regulation of actin microfilaments by human MICAL proteins. J Cell Sci 125 (2012) 614
-624
.

[20] I. Barravecchia, S. Mariotti, A. Pucci, F. Scebba, C. De Cesari, S. Bicciato, et al., MICAL2 is expressed in cancer associated neo-angiogenic capillary endothelia and it is required for endothelial cell viability, motility and VEGF response. Biochimica et Biophysica Acta (BBA) - Molecular Basis of Disease 1865 (2019) 2111-2124.

[21] X.L. Jia, S.Y. Li, S.S. Dang, Y.A. Cheng, X. Zhang, W.J. Wang, et al., Increased expression of chondroitin sulphate proteoglycans in rat hepatocellular carcinoma tissues. World J Gastroenterol 18 (2012) 3962-76.

[22] H. Yuan, B.L. Luo, B.M. He, [The effect of erythromycin on transforming growth factor-beta(1) and secretory leukocyte proteinase inhibitor in a rat model of chronic obstructive pulmonary disease]. Zhonghua Jie He He Hu Xi Za Zhi 34 (2011) 523-7.

[23] W. Yin, G. Tang, Q. Zhou, Y. Cao, H. Li, X. Fu, et al., Expression Profile Analysis Identifies a Novel Five-Gene Signature to Improve Prognosis Prediction of Glioblastoma. Front Genet 10 (2019).

[24] K. Friedrichs, S. Gluba, H. Eidtmann, W. Jonat, Overexpression of p53 and prognosis in breast cancer. Cancer-Am Cancer Soc 72 (1993) 3641-7.

[25] G.F. Ren, L. Tang, A.Q. Yang, W.W. Jiang, Y.M. Huang, Prognostic impact of NDRG2 and NDRG3 in prostate cancer patients undergoing radical prostatectomy. Histol Histopathol 29 (2014) 535-42.

[26] W. Wang, T. Shen, B. Dong, C.J. Creighton, Y. Meng, W. Zhou, et al., MAPK4 overexpression promotes tumor progression via noncanonical activation of AKT/mTOR signaling. J Clin Invest 129 (2019) 1015-1029.

[27] B. MacLean, D.M. Tomazela, N. Shulman, M. Chambers, G.L. Finney, B. Frewen, et al., Skyline: an open source document editor for creating and analyzing targeted proteomics experiments. Bioinformatics 26 (2010) 966-8.

[28] D. Gorlich, U. Kutay, Transport between the cell nucleus and the cytoplasm. Annu Rev Cell Dev Biol 15 (1999) 607-60.

[29] N. Kudo, N. Matsumori, H. Taoka, D. Fujiwara, E.P. Schreiner, B. Wolff, et al., Leptomycin B inactivates CRM1/exportin 1 by covalent modification at a cysteine residue in the central conserved region. Proc Natl Acad Sci U S A 96 (1999) 9112-7.

[30] S.D. Coaxum, J. Tiedeken, E. Garrett-Mayer, J. Myers, S.A. Rosenzweig, D.M. Neskey, The tumor suppressor capability of p53 is dependent on non-muscle myosin IIA function in head and neck cancer. Oncotarget 8 (2017) 22991-23007.

[31] Z. Xu, P. Li, D. Wei, Z. Wang, Y. Bao, J. Sun, et al., NMMHC-IIA-dependent nuclear location of CXCR4 promotes migration and invasion in renal cell carcinoma. Oncol Rep 36 (2016) 2681-2688.

[32] Y. Zhao, J. Wang, H. Jiang, Z. Yu, X. Li, J. Shi, Following OGD/R, annexin 1 nuclear translocation and subsequent induction of apoptosis in neurons are assisted by myosin IIA in a TRPM7 kinase-dependent manner. Mol Neurobiol 51 (2015) 729-42.

[33] D.G. Thomas, A. Yenepalli, C.M. Denais, A. Rape, J.R. Beach, Y. Wang, et al., Non-muscle myosin IIB is critical for nuclear translocation during 3D invasion. The Journal of Cell Biology 210 (2015) 583-594.

[34] Y. Huang, The angiogenic function of nucleolin is mediated by vascular endothelial growth factor and nonmuscle myosin. Blood 107 (2006) 3564-3571.

[35] 2016 Alzheimer's disease facts and figures. Alzheimers Dement 12 (2016) 459-509.

[36] M. Reck, D.F. Heigener, T. Mok, J.C. Soria, K.F. Rabe, Management of non-small-cell lung cancer: recent developments. Lancet 382 (2013) 709-19.

[37] S. Ashida, M. Furihata, T. Katagiri, K. Tamura, Y. Anazawa, H. Yoshioka, et al., Expression of novel molecules, MICAL2-PV (MICAL2 prostate cancer variants), increases with high Gleason score and prostate cancer progression. Clin Cancer Res 12 (2006) 2767-73.

[38] E. Psichari, A. Balmain, D. Plows, V. Zoumpourlis, A. Pintzas, High Activity of Serum Response Factor in the Mesenchymal Transition of Epithelial Tumor Cells Is Regulated by RhoA Signaling. J Biol Chem 277 (2002) 29490-29495.

[39] K. Katono, Y. Sato, S. Jiang, M. Kobayashi, R. Nagashio, S. Ryuge, et al., Prognostic Significance of MYH9 Expression in Resected Non-Small Cell Lung Cancer. Plos One 10 (2015) e0121460.

[40] B. Wang, X. Qi, J. Liu, R. Zhou, C. Lin, J. Shangguan, et al., MYH9 Promotes Growth and Metastasis via Activation of MAPK/AKT Signaling in Colorectal Cancer. J Cancer 10 (2019) 874-884.

[41] Y. Liu, Q. Jiang, X. Liu, X. Lin, Z. Tang, C. Liu, et al., Cinobufotalin powerfully reversed EBV-miR-BART22-induced cisplatin resistance via stimulating MAP2K4 to antagonize

non-muscle myosin heavy chain IIA/glycogen synthase 3beta/beta-catenin signaling pathway. Ebiomedicine (2019).

[42] B. Zhao, Z. Qi, Y. Li, C. Wang, W. Fu, Y.G. Chen, The non-muscle-myosin-II heavy chain Myh9 mediates colitis-induced epithelium injury by restricting Lgr5+ stem cells. Nat Commun 6 (2015) 7166.

[43] K. Reville, J.K. Crean, S. Vivers, I. Dransfield, C. Godson, Lipoxin A4 redistributes myosin IIA and Cdc42 in macrophages: implications for phagocytosis of apoptotic leukocytes. J Immunol 176 (2006) 1878-88.

[44] C. Perez-Ramirez, M. Canadas-Garre, M.A. Molina, M.J. Faus-Dader, M.A. Calleja-Hernandez, PTEN and PI3K/AKT in non-small-cell lung cancer. Pharmacogenomics 16 (2015) 1843-62.

[45] O. David, H. LeBeau, A.R. Brody, M. Friedman, J. Jett, Phospho-Akt overexpression in non-small cell lung cancer confers significant stage-independent survival disadvantage. Chest 125 (2004) 152S.

[46] S. Wang, Y. Zheng, Z. He, W. Zhou, Y. Cheng, C. Zhang, SH2B1 promotes NSCLC cell proliferation through PI3K/Akt/mTOR signaling cascade. Cancer Cell Int 18 (2018) 132.

[47] W. Li, C. Peng, M.H. Lee, D. Lim, F. Zhu, Y. Fu, et al., TRAF4 is a critical molecule for Akt activation in lung cancer. Cancer Res 73 (2013) 6938-50.

[48] X. Fu, C. Liang, F. Li, L. Wang, X. Wu, A. Lu, et al., The Rules and Functions of Nucleocytoplasmic Shuttling Proteins. Int J Mol Sci 19 (2018) 1445.

[49] X.H. Wei, S.S. Lin, Y. Liu, R.P. Zhao, G.J. Khan, Du HZ, et al., DT-13 attenuates human lung cancer metastasis via regulating NMIIA activity under hypoxia condition. Oncol Rep 36 (2016) 991-9.

[50] R.R. Bowers, Y. Manevich, D.M. Townsend, K.D. Tew, Sulfiredoxin Redox-Sensitive Interaction with S100A4 and Non-Muscle Myosin IIA Regulates Cancer Cell Motility. Biochemistry-Us 51 (2012) 7740-7754.

[51] S.S.P. Giridharan, J.L. Rohn, N. Naslavsky, S. Caplan, Differential regulation of actin microfilaments by human MICAL proteins. J Cell Sci 125 (2012) 614-24.

[52] M. Peckham, How myosin organization of the actin cytoskeleton contributes to the cancer phenotype. Biochem Soc T 44 (2016) 1026-1034.

[53] V. Betapudi, Myosin II motor proteins with different functions determine the fate of lamellipodia extension during cell spreading. Plos One 5 (2010) e8560.

[54] E.E. Grintsevich, H.G. Yesilyurt, S.K. Rich, R. Hung, J.R. Terman, E. Reisler, F-actin dismantling through a redox-driven synergy between Mical and cofilin. Nat Cell Biol 18 (2016) 876-885.

Figure Legends

Fig 1. Immunohistochemical analysis of MICAL2 expression in LUADs and paired normal lung tissues and its relationship to clinicopathological characteristics: A. MICAL2 expression levels are relatively lower in normal lung tissues and solely located in the nucleus, while it is highly expressed in LUADs and is mainly located in the cytoplasm. The MIOD of MICAL2 in LUADs is higher compared to paired normal lung tissues. In contrast to paired normal lung tissues, most LUADs have lower nuclear IRSs yet higher cytoplasmic IRSs. B. MICAL2 expression is higher in LUADs with lymphatic metastasis than in LUADs without lymphatic metastasis. Compared with non-lymphatic-metastasis LUADs, lymphatic-metastasis LUADs have higher total and cytoplasmic MICAL2 expression levels, while there is no significant difference in nuclear MICAL2 levels. C. Total and cytoplasmic MICAL2 expression levels, but not nuclear MICAL2 expression levels, in LUAD are related to poor prognosis.

Fig 2. MICAL2 promoted cell growth and metastasis in LUAD cell lines: A. MICAL2 is highly expressed in the PC-9 cell line while less expressed in the A549 cell line. B. RT-PCR or WB confirmed the knockdown or overexpression of MICAL2 expression levels in PC-9 or A549 cell lines. C. Representative images (gross and microscopic views) illustrate PC-9_nc, PC-9_sh1, and PC-9_sh3 cells as well as A549-CTRL and A549-MICAL2 cells in plate colony formation. Both PC-9_sh1 and PC-9_sh3 exhibit lower colony numbers and size compared to PC-9_nc (n = 3, *** = $P < 0.001$), while A549-MICAL2 exhibits colony numbers and size higher than A549-CTRL (n = 3, ** = $P < 0.01$, *** = $P < 0.001$). MICAL2-high cells were more epithelial-like compared to MICAL2-low cells based on the microscopic view. D. A CCK8 assay was used and absorbance at 450 nm (OD 450 nm) was measured (n = 4, ** = $P < 0.01$, *** = $P < 0.001$). E. Transwell assays with or without Matrigel showed that MICAL2 promotes migration and invasion in LUAD cells. Four fields (up, down, left, and right) were imaged and three independent assays were performed (n = 3, *** = $P < 0.001$, **** = $P < 0.0001$). F. Light microscopy images show the cellular morphological changes: the cells are epithelial-like (revealing the formation of

cobble stone-like cells and a reduction in protuberances) after MICAL2 was knocked down in PC-9 cells, while MICAL2-overexpressed A549 cells presented longer and more numerous protuberances compared with A549-CTRL cells. G. Knockdown of MICAL2 resulted in an increase in the epithelial markers ZO-1 and E-cadherin but decrease in the mesenchymal markers vimentin and β-catenin as well as myosin-9 and phosphorylation levels of AKT and PGSK-3β, while the overexpression of MICAL2 in A549 cell lines exhibited the opposite change in those markers. Right is the quantitative analysis of the bands (n = 3, * = $P < 0.05$, ** = $P < 0.01$, *** = $P < 0.001$).

Fig 3. MICAL2 shuttled between the cytoplasm and the nucleus: A. MICAL2 accumulated in the nucleus in PC-9 cells after treatment with LMB. The bottom panel shows nuclear and cytoplasmic positive rates of endogenous MICAL2: the nuclear positive rate dramatically increased after LMB treatment. B. Both nuclear and cytoplasmic localization of exogenous MICAL in A549-MICAL2 cells without LMB treatment, compared to a strong nuclear localization when treated with LMB. The bottom panel shows that the MICAL2 cytoplasmic positive rate was significantly decreased after LMB treatment. C. MICAL2 locations in HeLa cells transfected with WT and three truncated mutants of MICAL2. The right panel reveals a significant decrease in MICAL2 cytoplasmic positive rate in both MICAL2$^{-\Delta C}$ and MICAL2$^{-\Delta C\Delta N}$ transfected cells but not MICAL2$^{-\Delta N}$ transfected cells compared with MICAL2-WT transfected cells.

Fig 4. Myosin-9 bound to MICAL2 and its inhibition or knockdown negatively affected MICAL2 nuclear export: A. LC-MS/MS spectrum of the tryptic peptide LQQELDDLLVDLDHQR for myosin-9. Three independent IP-MS assays were performed in the PC-9 cell line using anti-MICAL2 antibody for detecting potential endogenously MICAL2-binding protein. B. IP-PRM (Parallel reaction monitoring) data for the sequence LPSPDPAASSSPSTVDSASPAR for MICAL2. The chromatographic traces show the overlapping transitions and retention time of the endogenous peptide of MICAL2. Three independent IP-PRM assays were performed in the PC-9 cell line using anti-myosin-9 antibody for exclusively detecting MICAL2-binding. C. HEK293T cells

were transfected with myosin-9-Flag and MICAL2-HA plasmid (left) or myosin-9-HA and MICAL2-Flag plasmid with control siRNA or si-myosin-9 (right). Immunoprecipitations were performed using an Anti-Flag M2 Affinity Gel. The immunoprecipitation products (IP) and total lysis (TL) were detected via western blotting (WB), which showed that MICAL2 and myosin-9 can bind to each other and the use of si-myosin-9 can inhibit the expression of myosin-9 as well as its binding capacity to MICAL2. D. Subcellular localizations of exogenous MICAL2 in A549-MICAL2 cells treated with or without ML7 or si-myosin-9. The positive rate of cytoplasmic MICAL2 decreased significantly after treatment.

Fig 5. Compared to MICAL2, MICAL2$^{-\Delta C}$ had less promoting effect on proliferation and mobility in LUAD cells *in vitro* and metastasis *in vivo*: A. MICAL2$^{-\Delta C}$ and MICAL2 were expressed in transfected A549 cells. Myosin-9 was enhanced in both A549-MICAL$^{-2\Delta C}$ and A549-MICAL2 cells compared with A549-CTRL cells. B. A549-MICAL2ΔC showed a significant increase in proliferation compared with A549-CTRL, while at a significantly lower level compared with A549-MICAL2 cells. C. The cell migration (top) and invasion (bottom) assays indicated that MICAL$^{-2\Delta C}$ did not promote migration or invasion in A549 cells as in MICAL2-WT cells. D. Representative images of lung metastatic nodules (circles marked with part of tumor metastatic focus) derived from A549 cells with or without stably overexpressing MICAL-$^{2\Delta C}$ or MICAL2. A549-MICAL2 showed a significant increase in metastatic nodule number while A549-MICAL2ΔC did not (n = 4, *** = $P < 0.001$).

Fig 6. Restraint of MICAL2 nuclear export inhibited the proliferation, migration, and invasion in LUAD cells: ML7 (A), LMB (B), and si-myosin-9 (C) inhibited the proliferation of both A549-MICAL2 and A549-CTRL cells at a significantly higher rate in the MICAL2-overexpressed A549 cells. A549-MICAL2 and A549-CTRL were inhibited in both migration capacity (D, F) and invasiveness (E, G) by ML7, LMB, or si-Myosin-9. The inhibition rates in A549-MICAL2 were significantly higher than in A549-CTRL after treatment.

Fig. S1 Modification of MICAL2 expression changed the morphology of LUAD cells. Cytoskeleton staining

with phalloidin showed that the knockdown of MICAL2 in PC-9 cells decreased the number of protuberances, while overexpression of MICAL2 in A549 cells increased the number of protuberances.

Fig. S2 Correlation of the expression and subcellular location between MICAL2 and myosin-9 LUAD tissues. A. *MYH9* mRNA expression [RNA Seq, log2(norm count +1] correlated with *MICAL2* mRNA expression [RNA Seq, log2(norm count +1)] across TCGA LUAD tissues. B. Both the total expression level and the cytoplasmic level of MICAL2 were positively associated with the myosin-9 expression level. The subcellular location of MICAL2 and myosin-9 were in accordance and the relevance of the cytoplasmic ratio of MICAL2 and myosin-9 was calculated.

Table 1. Association between MICAL2 protein expression and the clinical pathological characteristics of patients with LUADs

Pathological category		n	MI(IOD/AREA) Mean±SD	*P*	IRS of Cytoplasmic MICAL2 Negative	Positive	*P*	IRS of Nuclear MICAL2 Negtive	Positve	*P*
Total		126	0.106±0.049		24	102		86	40	
Sex	Male	74	0.109±0.052	0.4415	14	60	1.0000	50	24	1.0000
	Female	52	0.101±0.045		10	42		36	16	
Age	<60	67	0.113±0.047	0.0945	10	57	0.3561	45	22	0.8500
	≥60	58	0.098±0.051		13	45		40	18	
TNM	□	55	0.093±0.039	0.0163*	18	37	0.0026*	35	20	0.2603
	□	30	0.128±0.061		3	27		19	11	
	□~□	41	0.107±0.048		3	38		32	9	
T	1	39	0.099±0.036	0.5335	7	32	0.4529	26	13	0.6036
	2	61	0.110±0.058		14	47		44	17	
	3~4	26	0.104±0.046		3	23		16	10	
N	Negtive	74	0.095±0.042	0.0044*	24	50	< 0.0001*	46	28	0.0851
	Positive	52	0.120±0.053		0	52		40	12	
Differenciation	Well	19	0.081±0.043	0.0542	3	16	0.9177	14	5	0.7810
	Moderate	65	0.111±0.046		13	52		43	22	
	Poor	41	0.109±0.055		8	33		29	12	

* indicates $P < 0.05$

Table S1. Five most significant proteins interacted with MICAL2 detected by IP-MS using anti-MICAL2 antibody in PC-9 cells

Gene.names	Score	Intensity.a	Intensity.A	Intensity.b	Intensity.B	Intensity.c	Intensity.C	iBAQ	Rank	igG.1	Ab.1	igG.2	Ab.2	igG.3	Ab.3
MICAL2	323.31	0	8.28E+08	0	9.83E+08	0	8.42E+08	44216000	52	0	8.28E+08	0	9.83E+08	0	8.42E+0
YBX1	320.72	0	95837000	0	89311000	0	91619000	21290000	79	0	95837000	0	89311000	0	916190
RPL32	284.5	0	2.43E+08	0	3.96E+08	3001400	3.05E+08	1.35E+08	21	0	2.43E+08	0	3.96E+08	3001400	3.05E+0
RPL4	254.12	0	1.78E+08	0	1.66E+08	0	2.37E+08	36289000	60	0	1.78E+08	0	1.66E+08	0	2.37E+0
MYH9	249.05	0	70231000	0	93991000	0	82932000	2376500	188	0	70231000	0	93991000	0	829320

Table S2. Association between the clinical pathological characteristics and the combined expression of Myosin-9 and MICAL2 in LUAD.

			MICAL2	-	+		-		+	
Pathological category		n	Myosin-9	-	-	*P***	+	*P***	+	*P***
Total		74		17	10		14		33	
Sex	Male	39		7	4	1.0000	8	0.4795	20	0.2387
	Female	35		10	6		6		13	
Age	<60	47		13	6	0.0751	6	0.4147	22	0.5335
	≥60	27		4	8		4		11	
TNM	□~□	47		16	9	0.3846	9	0.0140*	13	<0.0001*
	□~□	27		0	1		5		21	
T	1~2	54		14	10	1.0000	8	0.4029	22	0.3274
	3~4	20		3	2		4		11	
N	Negtive	45		16	9	1.0000	10	0.1484	10	<0.0001*
	Positive	29		1	1		4		23	
Differenciation	Moderate~Well	43		10	6	1.0000	10	0.7074	17	0.7694
	Poor	30		7	4		4		15	

* indicates $P < 0.05$

**compared with the group of “MICAL2 - & Myosin-9 - “

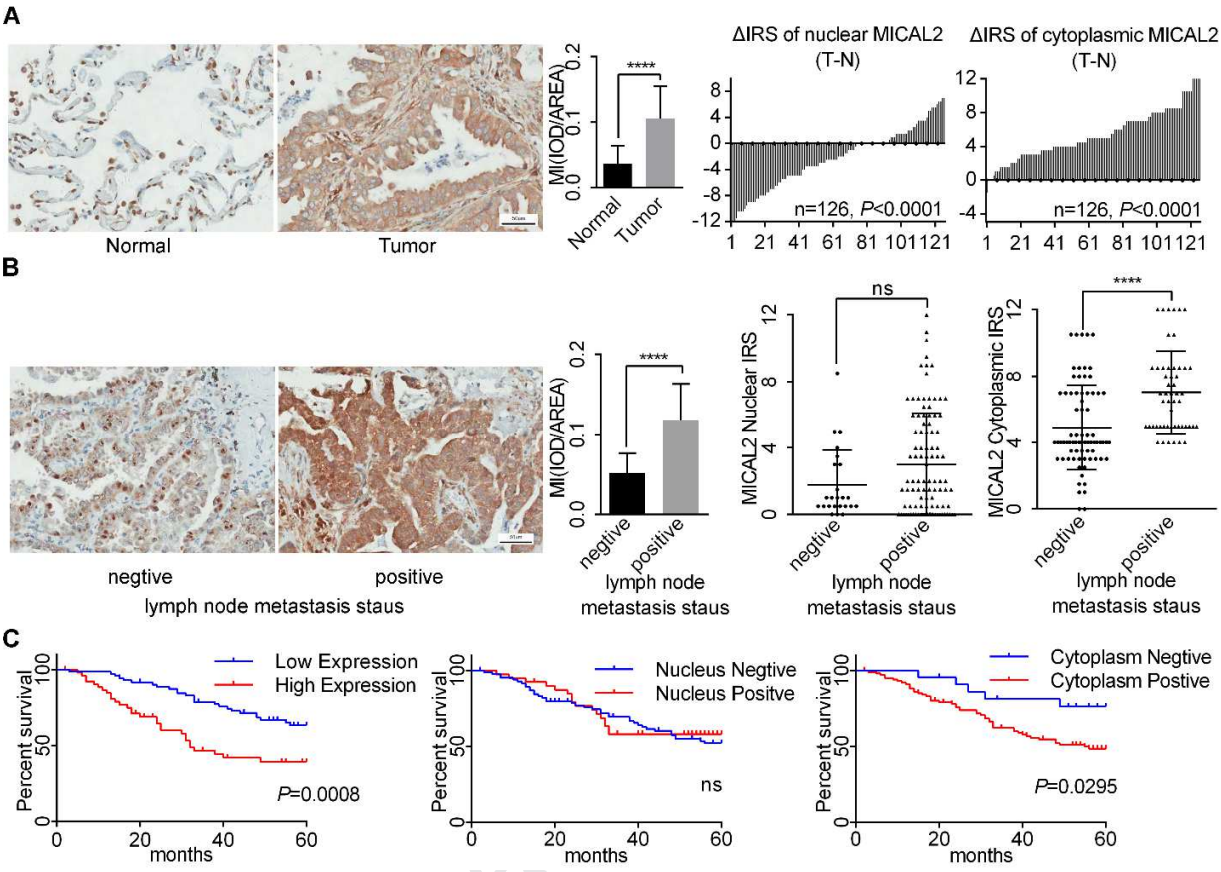

Fig. 1

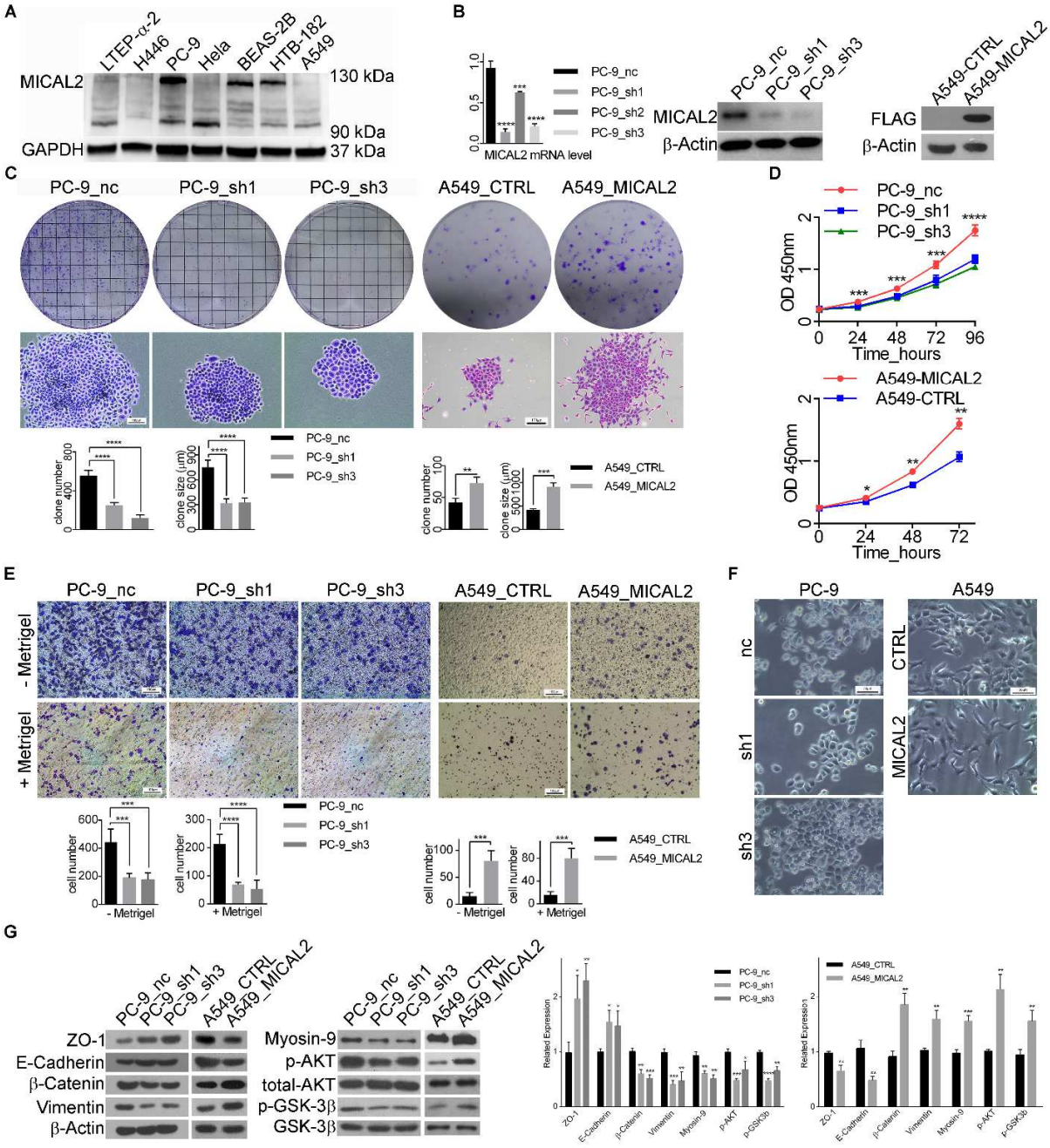
A
LTEP-α-2
H446
PC-9
Hela
BEAS-2B
HTB-182
A549
MICAL2
130 kDa
GAPDH
90 kDa
37 kDa
B
MICAL2 mRNA level
PC-9_nc
PC-9_sh1
PC-9_sh2
PC-9_sh3
MICAL2
β-Actin
FLAG
A549-CTRL
A549-MICAL2
C
PC-9_nc
PC-9_sh1
PC-9_sh3
A549_CTRL
A549_MICAL2
clone number
clone size (μm)
D
OD 450nm
Time_hours
E
- Metrigel
+ Metrigel
cell number
F
PC-9
A549
nc
sh1
sh3
CTRL
MICAL2
G
ZO-1
E-Cadherin
β-Catenin
Vimentin
β-Actin
Myosin-9
p-AKT
total-AKT
p-GSK-3β
GSK-3β
Related Expression

Fig. 2

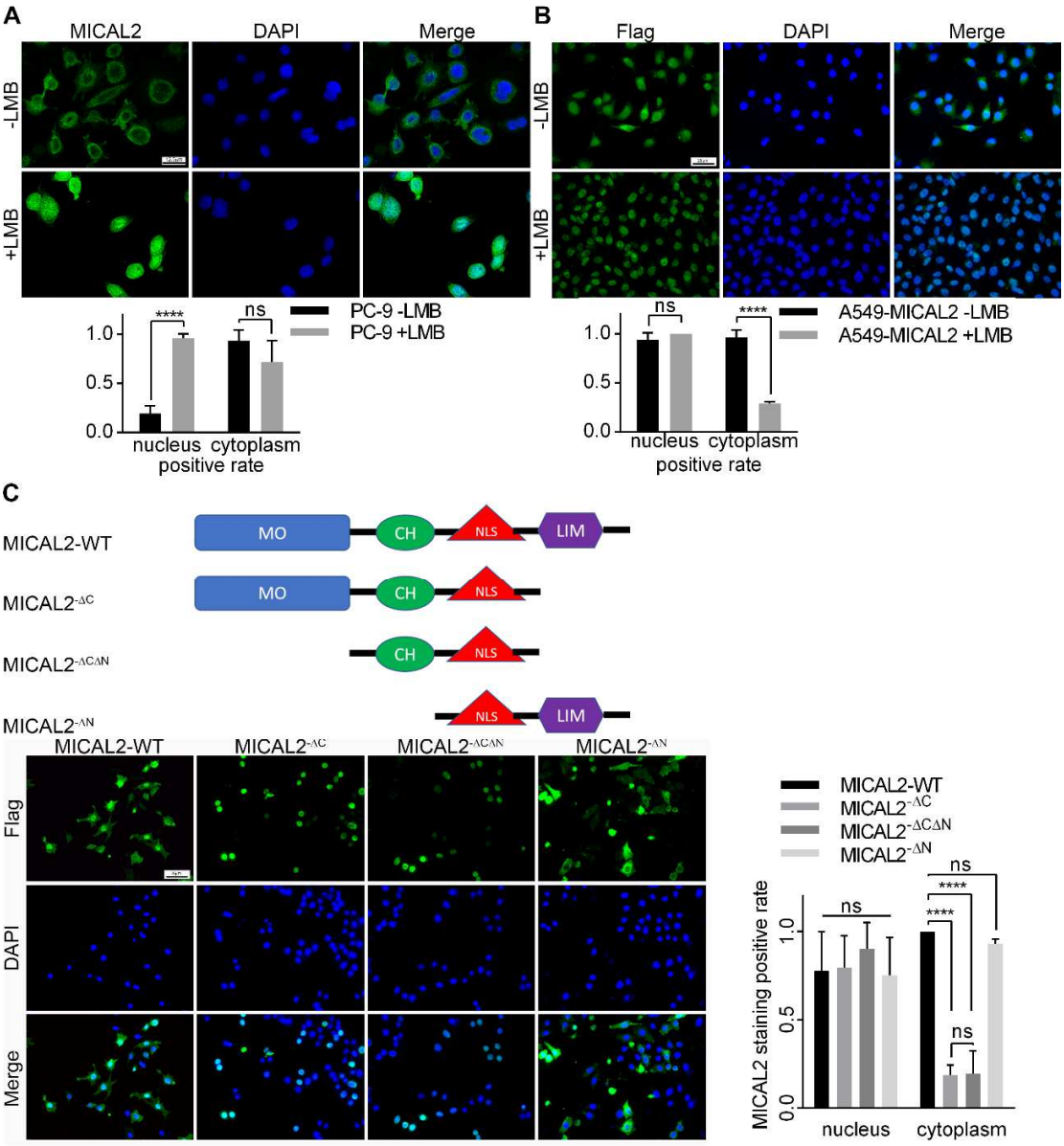
A
MICAL2
DAPI
Merge
-LMB
+LMB
****
ns
PC-9 -LMB
PC-9 +LMB
1.0
0.5
0.0
nucleus
cytoplasm
positive rate
B
Flag
DAPI
Merge
-LMB
+LMB
ns
****
A549-MICAL2 -LMB
A549-MICAL2 +LMB
1.0
0.5
0.0
nucleus
cytoplasm
positive rate
C
MICAL2-WT
MICAL2-ΔC
MICAL2-ΔCΔN
MICAL2-ΔN
MO
CH
NLS
LIM
MICAL2-WT
MICAL2-ΔC
MICAL2-ΔCΔN
MICAL2-ΔN
Flag
DAPI
Merge
MICAL2-WT
MICAL2-ΔC
MICAL2-ΔCΔN
MICAL2-ΔN
MICAL2 staining positive rate
ns
****
ns
****
ns
1.0
0.5
0.0
nucleus
cytoplasm

Fig. 3

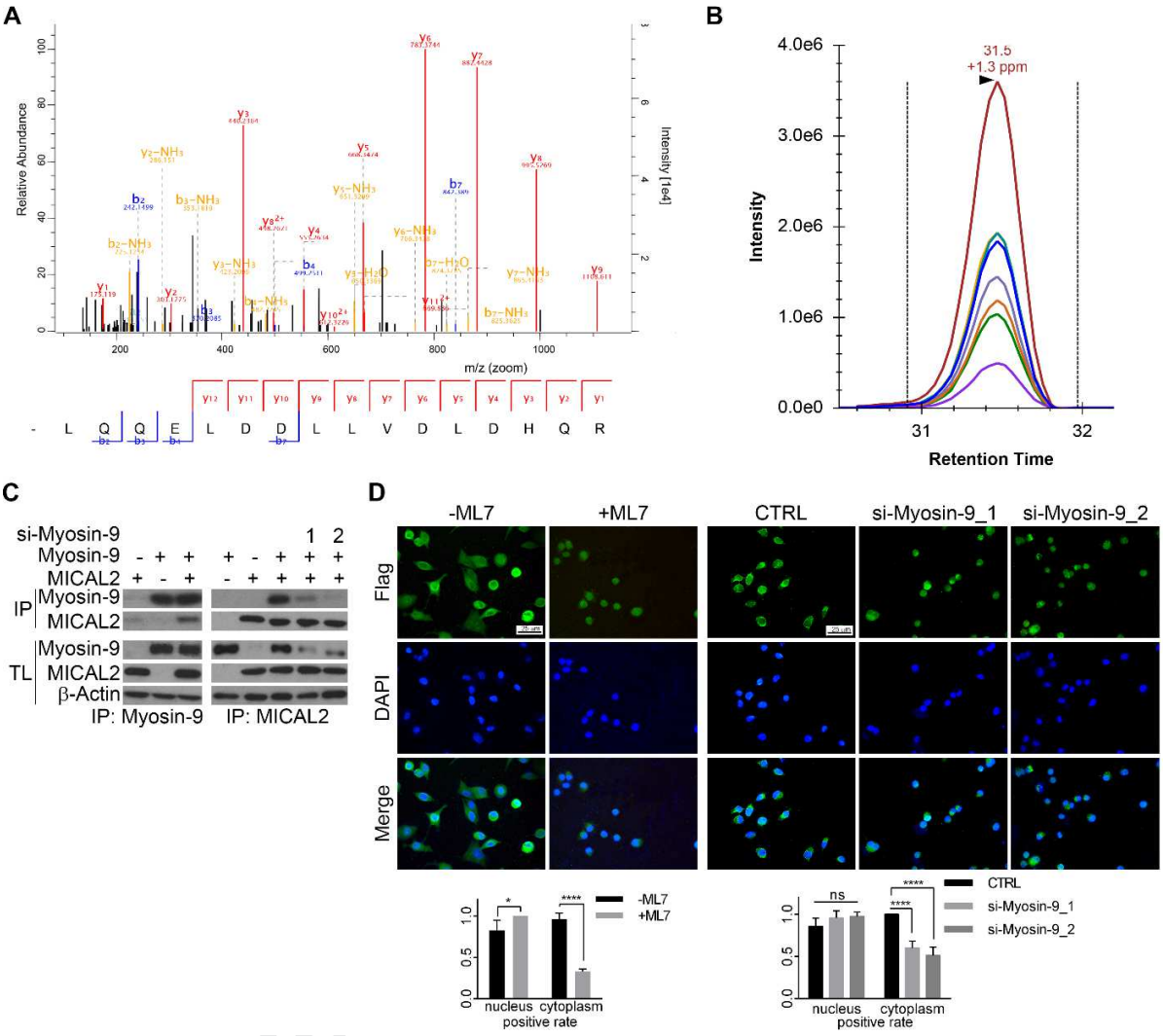
A
Relative Abundance
Intensity [1e4]
m/z (zoom)
- L Q Q E L D D L L V D L D H Q R
B
31.5
+1.3 ppm
Intensity
Retention Time
C
si-Myosin-9
Myosin-9
MICAL2
IP
TL
β-Actin
IP: Myosin-9
IP: MICAL2
D
-ML7
+ML7
CTRL
si-Myosin-9_1
si-Myosin-9_2
Flag
DAPI
Merge
nucleus
cytoplasm
positive rate
ns

Fig. 4

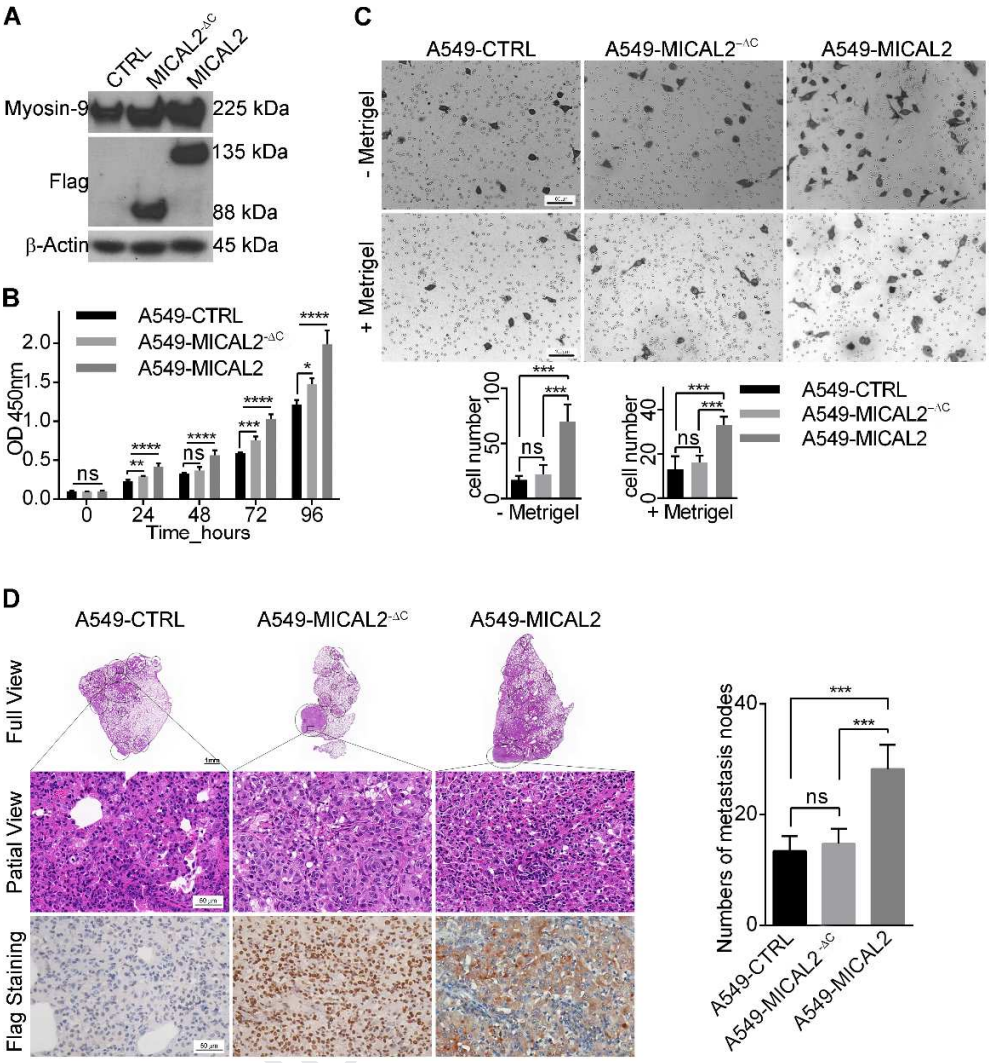
A
CTRL
MICAL2-ΔC
MICAL2
Myosin-9
225 kDa
Flag
135 kDa
88 kDa
β-Actin
45 kDa
B
A549-CTRL
A549-MICAL2-ΔC
A549-MICAL2
OD 450nm
Time_hours
C
A549-CTRL
A549-MICAL2-ΔC
A549-MICAL2
- Metrigel
+ Metrigel
cell number
D
A549-CTRL
A549-MICAL2-ΔC
A549-MICAL2
Full View
Patial View
Flag Staining
Numbers of metastasis nodes

Fig. 5

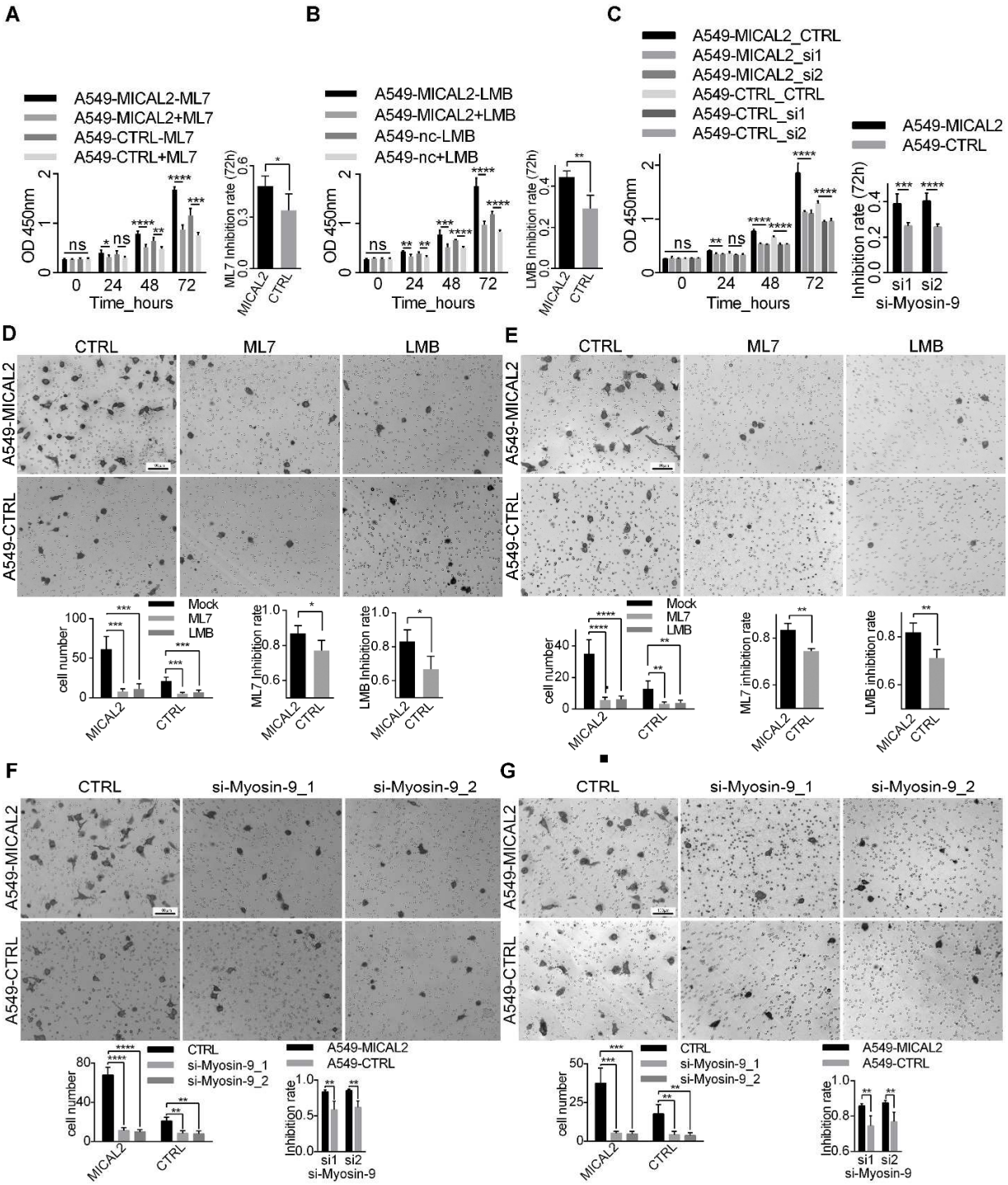
A
A549-MICAL2-ML7
A549-MICAL2+ML7
A549-CTRL-ML7
A549-CTRL+ML7
OD 450nm
Time_hours
ML7 Inhibition rate (72h)
MICAL2
CTRL
B
A549-MICAL2-LMB
A549-MICAL2+LMB
A549-nc-LMB
A549-nc+LMB
LMB Inhibition rate (72h)
C
A549-MICAL2_CTRL
A549-MICAL2_si1
A549-MICAL2_si2
A549-CTRL_CTRL
A549-CTRL_si1
A549-CTRL_si2
A549-MICAL2
A549-CTRL
Inhibition rate (72h)
si1
si2
si-Myosin-9
D
CTRL
ML7
LMB
A549-MICAL2
A549-CTRL
Mock
cell number
E
F
si-Myosin-9_1
si-Myosin-9_2
G

Fig. 6

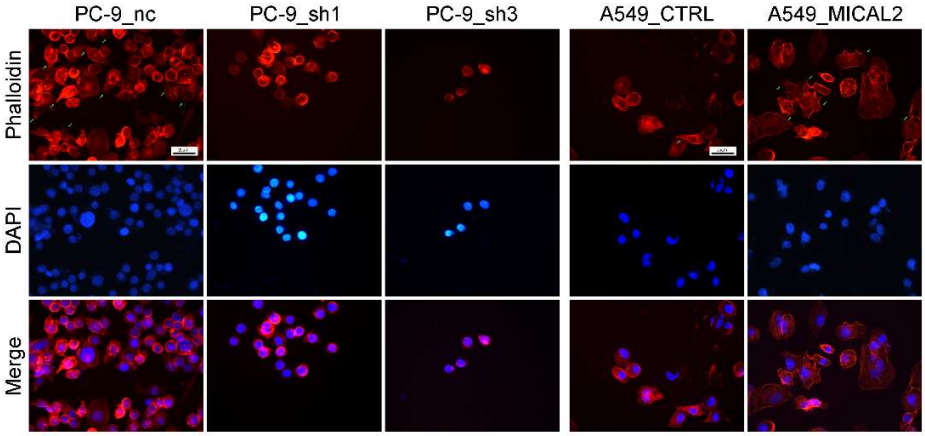
PC-9_nc
PC-9_sh1
PC-9_sh3
A549_CTRL
A549_MICAL2
Phalloidin
DAPI
Merge

Fig. S1

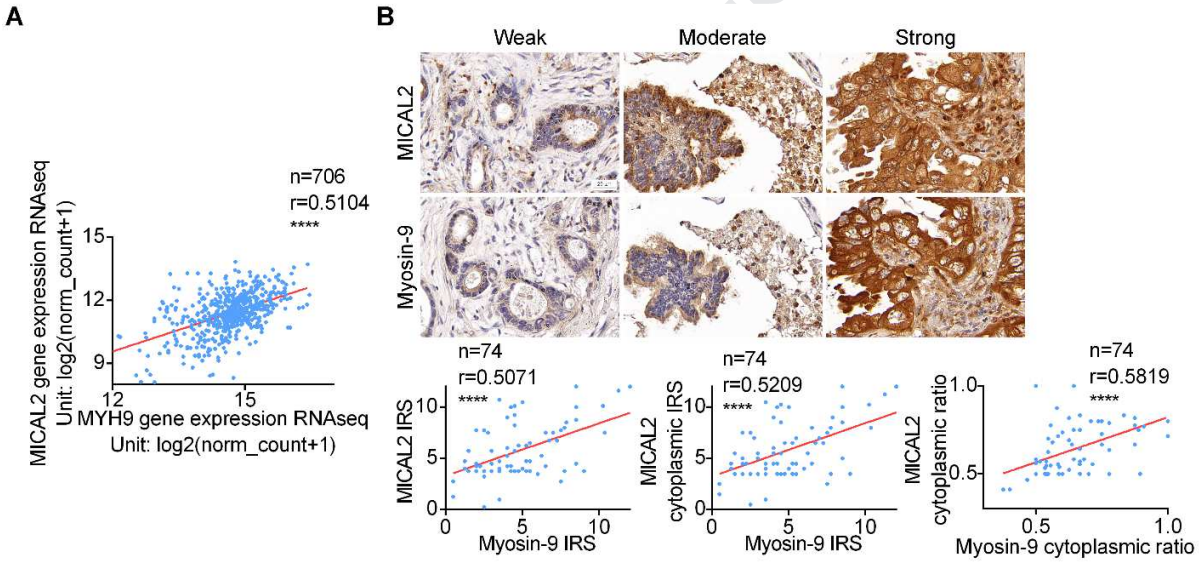
A
n=706
r=0.5104
****
MICAL2 gene expression RNAseq
Unit: log2(norm_count+1)
MYH9 gene expression RNAseq
Unit: log2(norm_count+1)
B
Weak
Moderate
Strong
MICAL2
Myosin-9
n=74
r=0.5071
****
MICAL2 IRS
Myosin-9 IRS
n=74
r=0.5209
****
MICAL2 cytoplasmic IRS
Myosin-9 IRS
n=74
r=0.5819
****
MICAL2 cytoplasmic ratio
Myosin-9 cytoplasmic ratio

Fig. S2

Highlights:

- MICAL2 promotes cancer invasion and growth of lung adenocarcinoma.
- MICAL2 was overexpressed and cytoplasm-enriched in LUAD tissues.
- MICAL2 promotes LUAD cell proliferation, migration, invasion, and EMT.
- MICAL2 was proved to be a nucleocytoplasmic shuttling protein regulated by myosin-9.
- MICAL2 overexpression and nuclear export were associated with cancer progression.

Conflicts of interest

The authors declare that they have no conflicts of interest.